High-temperature expansion method for calculating paramagnetic exchange interactions

O. M. Sotnikov and V. V. Mazurenko

Theoretical Physics and Applied Mathematics Department, Ural Federal University, Mira Str. 19, 620002 Ekaterinburg, Russia

(Received 13 January 2016; published 2 November 2016)

The method for calculating the isotropic exchange interactions in the paramagnetic phase is proposed. It is based on the mapping of the high-temperature expansion of the spin-spin correlation function calculated for the Heisenberg model onto the Hubbard Hamiltonian one. The resulting expression for the exchange interaction has a compact and transparent formulation. The quality of the calculated exchange interactions is estimated by comparing the eigenvalue spectra of the Heisenberg model and low-energy magnetic part of the Hubbard model. By the example of quantum rings at half-filling with different hopping setups, we analyze contributions from different parts of the Hubbard model spectrum to the resulting exchange interaction. The developed method can be applied for simulating magnetic couplings in correlated materials and surface nanostructures.

DOI: 10.1103/PhysRevB.94.195107

I. INTRODUCTION

The magnetic properties of a correlated system can be fully described by its magnetic susceptibility characterizing the response of the system to an external magnetic field [1]. Modern numerical methods of the dynamical mean-field theory for solving realistic electronic models provide the most reliable information concerning the electronic and magnetic excitation spectra of the strongly correlated materials. Importantly, by using the dynamical mean-field theory [2] (DMFT), the frequency- and momentum-dependent susceptibilities of a correlated material can be directly calculated at different external parameters (temperatures and magnetic fields) and compared with those measured in the experiment. However, the solution and reproduction of the experimentally observed susceptibilities do not mean a truly microscopic understanding of the magnetic properties formation. In this respect, the determination of the individual magnetic interactions J_{ij} of the Heisenberg model is of crucial importance. The corresponding Hamiltonian is given by

$$\hat{H}_{\text{Heis}} = \sum_{ij} J_{ij} \hat{\vec{S}}_i \hat{\vec{S}}_j. \tag{1}$$

The development of the methods for calculating the exchange interactions J_{ij} between magnetic moments in modern materials is an active research field [3–6]. Some important examples of such methods are listed in Table I. They are generally applicable to periodic complex multiband systems with various magnetic and nonmagnetic species. In contrast, being formulated for finite clusters the method we present in this paper can be applied to the investigation of the magnetic couplings in magnetic molecules or nanostructures deposited on the insulating and metallic surfaces. Below we shortly describe and compare different approaches.

The density-functional exchange formula proposed in Ref. [6] is based on the idea about infinitesimal rotation of the magnetic moments from the collinear ground state. The resulting exchange interaction is the response of the system on this perturbation. Being formulated in terms of the Green's function of the system, such an approach has a number of important options, for instance, it is possible to calculate the orbital contributions to the total exchange interaction. The latter opened a way for a truly microscopic analysis of the magnetic couplings.

Then, in Ref. [3] the method for calculating magnetic couplings within the LDA+DMFT scheme was reported. Such an approach facilitates the analysis of the exchange interactions taking the dynamical Coulomb correlations into account [7–11]. Recently, a general technique to extract the complete set of the magnetic couplings by taking into account the vertices of two-particle Green's functions and nonlocal self-energies was developed in Ref. [5].

By construction, the methods reviewed above assume some type of the magnetic ordering in the system. Thus, another important methodological problem in this research field concerns the determination of the magnetic couplings in a system being in a disordered magnetic phase. For that, a formulation in terms of generalized perturbation method of the disordered local moment approach was proposed [15,16]. This approach works quite well for the exchange parameters, the Curie temperature, and energetics for the planar spin spirals in the $3d$ magnets (Fe, Co, and Ni). One of the advantages of the generalized perturbation method is the possibility to calculate the high-order terms of the Heisenberg model.

Numerous magnetic experiments [17–19] revealed quantum spin systems, which, due to the low-dimensional crystal structure, do not exhibit any sign of the magnetic ordering, even at *very low temperatures*. Since the electron hopping integral t_{ij} in these materials is much smaller than the onsite Coulomb interaction U, then the magnetic coupling can be associated with the Anderson's superexchange interaction [13] $J_{ij} = \frac{4t_{ij}^2}{U}$. For intermediate values of t/U ($\sim$0.1), one can still use the pure spin model with parameters defined from the high-order strong coupling expansion within perturbative continuous unitary transformations [20,21].

In turn, the simulation of the exchange interactions in high-temperature paramagnetic phases can be performed by means of the dynamical mean-field theory and its extension. For instance, in case of the γ iron, the authors of Ref. [22] compared the magnetic susceptibilities obtained for Heisenberg model within $1/z$ expansion and that calculated in DMFT approach. To describe the formation of the local magnetic moment and exchange interaction in the α iron, a spin-fermion model was proposed in Ref. [23].

TABLE I. List of methods for calculation of the isotropic exchange interaction. $\phi_i(x)$ is a wave function centered at the lattice site i. t_{ij} and U are the hopping integral and the onsite Coulomb interaction, respectively. z is the number of the nearest neighbors. E_{FM} and E_{AFM} are the energies of the ferromagnetic and antiferromagnetic solutions obtained by using a mean-field electronic structure approach. $\Gamma_{ij}^{(1)}$ is the first-order term in the high-temperature expansion of the spin-spin correlation function.

Method	Expression
Heitler-London's exchange [12]	$J_{ij} = \int \frac{\phi_i^*(x)\phi_j(x)\phi_j^*(x')\phi_i(x')}{\lvert x-x'\rvert} dx\, dx'$
Anderson's superexchange theory [13]	$J_{ij}^{\mathrm{kin}} = \frac{4t_{ij}^2}{U}$
Total energies method [14]	$J = \frac{E_{\mathrm{FM}}-E_{\mathrm{AFM}}}{4zS^2}$
Local force theorem [6]	$J_{ij} = \frac{\partial^2 E}{\partial \vec{S}_i \partial \vec{S}_j}$
HTE method (this work)	$J_{ij} = -\frac{\Gamma_{ij}^{(1)}}{[\frac{1}{3}S(S+1)]^2}$

Here, we report on a distinct method, high-temperature expansion (HTE) method for calculating the isotropic exchange interactions in the paramagnetic phase. It is based on the mutual mapping of the high-temperature spin-spin correlation functions calculated in Hubbard and Heisenberg models. It can be also expanded on the calculation of the high-order couplings such as four-spin exchange. We have used the developed approach to study the magnetic interactions in quantum spin rings at half-filling (one doubly degenerate state per site) with different hopping configurations.

II. METHOD

The focus in our approach is concentrated on the spin-spin correlation function

$$\Gamma_{ij} = \frac{\mathrm{Tr}\left(\hat{S}_i^z \hat{S}_j^z e^{-\beta\hat{H}}\right)}{\mathrm{Tr}(e^{-\beta\hat{H}})}, \tag{2}$$

where β is the inverse temperature and $\hat{H}$ is the Hamiltonian describing the system in question. Since the paramagnetic regime is of our interest, then we can consider the z component of the spin operator. Following Ref. [24], we consider Γ_{ij} in the high-temperature limit in which the exponent is expanded as $e^{-\beta\hat{H}} = 1 - \beta\hat{H}$. Thus, one obtains

$$\Gamma_{ij} \approx \Gamma_{ij}^{(0)} + \beta\Gamma_{ij}^{(1)} = \frac{\mathrm{Tr}\left(\hat{S}_i^z \hat{S}_j^z\right) - \beta\mathrm{Tr}\left(\hat{S}_i^z \hat{S}_j^z \hat{H}\right)}{\mathrm{Tr}(1) - \beta\mathrm{Tr}(\hat{H})}, \tag{3}$$

where $\mathrm{Tr}(\hat{A})$ is the trace that corresponds to the summation over all eigenstates of the Hamiltonian of the system $\hat{H}$:

$$\mathrm{Tr}(\hat{\mathrm{A}}) = \sum_n \langle\Psi_n|\hat{A}|\Psi_n\rangle. \tag{4}$$

If the system in question can be described by the Heisenberg Hamiltonian with localized magnetic moments, then in zero order on β one obtains

$$\mathrm{Tr}\left(\hat{S}_i^z \hat{S}_j^z\right) = \tfrac{1}{3}S(S+1)N\delta_{ij}, \tag{5}$$

which simply means that the spins are independent at high temperatures. Here, $N = (2S+1)^L$ is the number of the eigenstates of the Heisenberg Hamiltonian (L denotes the number of sites in the model).

The same idea is used when analyzing the contribution of the first order on β to the spin-spin correlation function that carries the information concerning the exchange interaction between the spins:

$$\begin{aligned}\mathrm{Tr}\left(\hat{S}_i^z \hat{S}_j^z \hat{H}_{\mathrm{Heis}}\right) &= \mathrm{Tr}\left(\hat{S}_i^z \hat{S}_j^z \sum_{m\neq n} J_{mn} \hat{\vec{S}}_m \hat{\vec{S}}_n\right) \\ &= J_{ij}\mathrm{Tr}\left(\hat{S}_i^z \hat{S}_j^z \hat{S}_i^z \hat{S}_j^z\right) = J_{ij} N \left(\frac{1}{3}S(S+1)\right)^2.\end{aligned} \tag{6}$$

The detail derivation of Eqs. (5) and (6) is presented in Appendix A. This high-temperature decomposition of the spin-spin correlation function was used by the authors of Ref. [24] to obtain the expression for the Curie-Weiss temperature. As we will show below, it can be also used for calculating J_{ij}.

In the seminal work by Anderson [13], the Heisenberg exchange interaction is defined in terms of the Hubbard model parameters t_{ij} and U. For that, the author considered the limit $t_{ij} \ll U$, in which one can obtain the famous superexchange expression $J_{ij} = \frac{4t_{ij}^2}{U}$. Our method for calculating J_{ij} is also based on the using of the Hubbard model that in the simplest one-band form can be written as [25]

$$\hat{H}_{\mathrm{Hubb}} = \sum_{ij\sigma} t_{ij}\hat{c}_{i\sigma}^+ \hat{c}_{j\sigma} + \frac{U}{2}\sum_{i\sigma}\hat{n}_{i\sigma}\hat{n}_{i-\sigma} - \mu\sum_{i\sigma}\hat{n}_{i\sigma}, \tag{7}$$

where σ is the spin index, t_{ij} is the hopping integral between ith and jth sites, U is the onsite Coulomb interaction, and μ is the chemical potential.

Since our aim is to define the parameters of the Heisenberg model with localized spins, on the level of the Hubbard model it is natural to start with the atomic limit in which the hopping integral is much smaller than the Coulomb interaction $U \gg t$. In this case, the spectrum of the eigenvalues can be divided onto low- and high-energy parts that are related to the magnetic excitations of the Heisenberg type and charge excitations of the order of U, respectively. Our method is based on the comparison of the magnetic observables such as spin-spin correlation functions calculated in Hubbard model and Heisenberg model approaches in the high-temperature limit $\beta \to 0$.

In general, the trace over spin operators [Eq. (4)] differs in the case of the Heisenberg and Hubbard models. For instance, one should perform the summation over all eigenstates for the Heisenberg model. At the same time, in the case of the Hubbard model one should exclude the high-energy eigenstates with doubly occupied sites from the consideration. The energies of these states are of order of U.

In the limit of the localized spins $t \ll U$ that we consider, the traces $\mathrm{Tr}(\hat{S}_i^z \hat{S}_j^z)$ [in the numerator of Eq. (3)] and $\mathrm{Tr}(\hat{H})$ [in the denominator of Eq. (3)] are similar to that defined for the Heisenberg model. We are interested in the first-order term on

the inverse temperature for which one obtains

$$\mathrm{Tr}\big(\hat{S}_i^z \hat{S}_j^z \hat{H}_{\mathrm{Hubb}}\big) = \sum_{n=0}^{N-1} \langle \Psi_n | \hat{S}_i^z \hat{S}_j^z \hat{H}_{\mathrm{Hubb}} | \Psi_n \rangle = \sum_{n=0}^{N-1} E_n \langle \Psi_n | \hat{S}_i^z \hat{S}_j^z | \Psi_n \rangle, \quad (8)$$

where E_n is the eigenvalue of the Hubbard model, Ψ_n is the corresponding eigenvector, and N is the number of the eigenstates of the Heisenberg Hamiltonian.

Comparing Eqs. (6) and (8) one can derive the following expression for the Heisenberg's exchange interaction:

$$J_{ij} = \frac{\sum_{n=0}^{N-1} E_n \langle \Psi_n | \hat{S}_i^z \hat{S}_j^z | \Psi_n \rangle}{N\left[\frac{1}{3}S(S+1)\right]^2}. \quad (9)$$

Let us analyze the obtained expression for the paramagnetic exchange interaction. First of all, it contains the summation over all eigenstates belonging to the magnetic part of the full Hubbard spectrum. The high-energy part of the Hubbard spectrum describing the charge excitations is excluded from the consideration. For each eigenstate, we measure the correlation between two spins. Such a correlation can be positive or negative depending on the spin configuration encoded in the eigenstate and is multiplied by the excitation energy with respect to the ground state with $E_0 = 0$.

Limitations of the method. The expression for the exchange interaction (9) was obtained by comparing the spin-spin correlation functions of the Heisenberg and Hubbard models in the limit $t \ll U$. In this regime, the low-energy magnetic part of the Hubbard model eigenspectrum is separated from the high-energy one describing the charge excitations. Such separation plays a crucial role and defines the playground for our method. Practically, it means that all the simulations of the magnetic couplings and excitation spectra presented in this paper were performed for the ratio $\frac{t}{U}$ at which the magnetic part is not mixed with the charge one. It ensures the mapping of the spin-spin correlation functions described above and truncation of the Hubbard spectrum in Eq. (9). In Appendix C, we consider a five-site spin ring beyond the critical ratio of $\frac{t}{U}$ where intersection between magnetic and electronic parts of spectrum occurs.

Importantly, there are some cases, as we will show below, when such a separation exists even at $\frac{t}{U} \sim 1$, which leads to agreement of the Heisenberg and Hubbard eigenvalue spectra. It means that we can analyze the magnetic interactions in the strongly correlated regime.

For transition-metal oxides, the typical ratio between hopping integral and onsite Coulomb interaction is of order of 0.03. It was shown that in case of $5d$ iridium oxides [26], this value can be about two times larger, 0.07, and the implementation of the ordinary superexchange theory is questionable. The simulation of the magnetic interaction in metallic systems is another complicated problem, one deals with the situation when the hopping integrals are of the same order of magnitude as the Coulomb interaction.

One important problem when calculating the exchange interaction is how to estimate and control the quality of the obtained exchange interactions. It can be done by solving the corresponding Heisenberg model and by calculating the experimentally observed quantities (such as magnetic susceptibility, magnetization, and other). The comparison of the calculated theoretical dependencies with the available experimental data is a standard way to define the reliability of the constructed Heisenberg model. In our study, the exchange interactions for the spin model estimated on the basis of the electronic Hubbard Hamiltonian. Thus, it is natural to estimate the quality of the constructed Heisenberg model by comparing the eigenvalue spectra of the spin model and parent electronic Hamiltonian at different degree of the localization.

Extension to many-orbital systems. In the case of the many-band Hubbard model, the spin operator of the ith site in Eq. (9) can be written as the sum of the orbital contributions [27] $\hat{S}_i^z = \sum_m \hat{S}_{i,m}^z$. Thus, for the $S > \frac{1}{2}$ we obtain the following expression for the paramagnetic exchange interaction

$$J_{ij} = \frac{\sum_{mm'} \sum_{n=0}^{N-1} E_n \langle \Psi_n | \hat{S}_{i,m}^z \hat{S}_{j,m'}^z | \Psi_n \rangle}{N\left[\frac{1}{3}S(S+1)\right]^2}. \quad (10)$$

Other types of the reference Hamiltonians. Importantly, the realization of our method is not limited by the Hubbard model for finite clusters. One can use other types of the strongly correlated Hamiltonians to define the spin-spin correlation functions. For instance, it can be the Anderson model [13] that is widely used for simulation of the correlated nanostructures on a surface [28–30]. In this case, the E_n and Ψ_n in Eq. (9) are the eigenvalues and eigenfunctions of Anderson model Hamiltonian. In Sec. IV, we discuss the dependence of the exchange interaction in the dimer on hybridization strength with a surface. The combination of the developed approach with Anderson impurity solver facilitates the realization of our method within the LDA+DMFT scheme, which opens a way for simulating exchange interaction in periodic systems.

III. EXACT SOLUTION FOR DIMER

The electronic and magnetic excitation spectra of the dimer that can be obtained analytically is the classical test in the field of the strongly correlated materials. Importantly, there are a lot of examples of the real low-dimensional materials that have the dimer motif. For instance, they are vanadium and copper oxides with d^1 and d^9 atomic configurations [31–33]. The superexchange interaction in the dimer can be also simulated within the experiments with ultracold atoms in optical lattice [34]. In such experiments, the hopping integral and onsite Coulomb interaction can be varied in a wide range. For instance, the authors of Ref. [35] explored the ratios ranging from the metallic ($t/U \sim 0.1$) to insulating ($t/U \ll 1$) regimes when performing the quantum simulations on the two-dimensional optical lattice.

Within the proposed method we are interested in $N = 4$ lowest magnetic eigenstates of the Hubbard model; they are presented in Table II, where the following notations are used: $C_0^2 = \frac{1}{2(1+\epsilon_-^2)}$, $\epsilon_- = \frac{U(1-\gamma)}{4t}$, $\gamma = \sqrt{1 + \frac{16t^2}{U^2}}$. The eigenvalues are the following: $E_0 = \frac{U}{2}(1-\gamma) - 2\mu$, $E_1 = E_2 = E_3 = -2\mu$. The solution of the dimer model can be found in the literature [36].

TABLE II. Four lowest eigenstates of the Hubbard model for the dimer.

n	Ψ_n
0	$[(\lvert\downarrow\uparrow\rangle - \lvert\uparrow\downarrow\rangle) + \frac{U(1-\gamma)}{4t}(\lvert\downarrow\uparrow,-\rangle + \lvert-,\downarrow\uparrow\rangle)]C_0$
1	$\lvert\uparrow\uparrow\rangle$
2	$\lvert\downarrow\downarrow\rangle$
3	$\frac{1}{\sqrt{2}}(\lvert\uparrow\downarrow\rangle + \lvert\downarrow\uparrow\rangle)$

By using the developed method (9), we obtain the following exchange interaction in the dimer:

$$J = -\frac{U}{2}(1-\gamma). \tag{11}$$

This value is exactly the excitation energy from the singlet to triplet state of the dimer $E_1 - E_0$. Thus, in case of isolated dimer, our method can be used to construct a Heisenberg model reproducing the Hubbard model spectrum for any reasonable ratio of kinetic and Coulomb interaction parameters $\frac{t}{U}$ (Fig. 1). On the other hand, the Heisenberg model constructed by means of the Anderson's superexchange theory $J = \frac{4t^2}{U}$ results in the spectrum deviating from that of the original Hubbard model at $\frac{t}{U} > 0.2$.

A. Comparison with the Hartree-Fock solution

One of the important results of modern magnetism theory was the development of the local force theorem [6] for calculating the exchange interactions. Such an approach gives reliable results and is widely used for simulation magnetic properties of the transition-metal compounds [7–10,26]. Thus, the next step of our investigation was to compare the results of the high-temperature expansion method we developed and those obtained by using the density-functional exchange formula. For these purposes, we have chosen the dimer system.

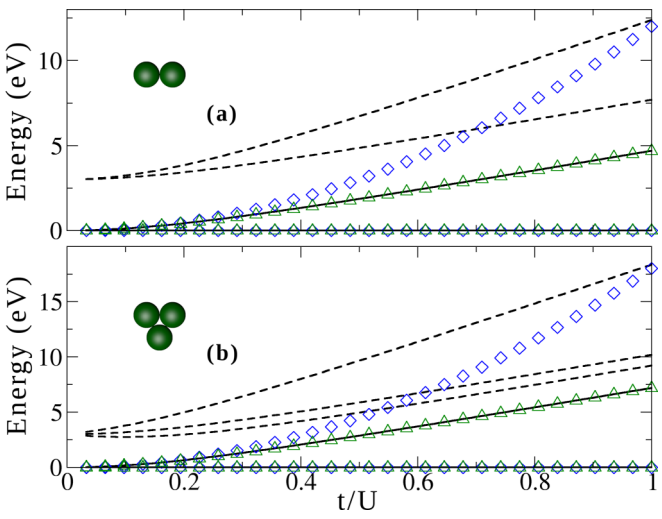

FIG. 1. Comparison of the excitation spectra of the Hubbard model (solid and dashed lines) and Heisenberg models with exchange interaction calculated by using the developed method (green triangles) and superexchange Anderson approach (blue rhombus) for isolated (a) dimer and (b) triangle.

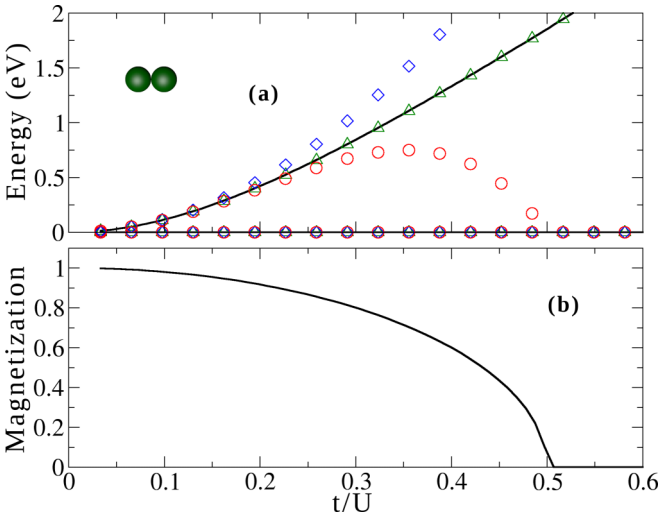

FIG. 2. (a) Comparison of the eigenvalue spectra obtained from the solution the Hubbard model (black solid line) and the Heisenberg models with parameters calculated by the developed approach (9) (green triangles), local force theorem method (13) (red circles), and Anderson's superexchange theory (blue rhombus). (b) Magnetization as a function of the localization.

Since the method based on the local force theorem requires a nonzero magnetization of the system, we used the Hartree-Fock approximation to solve the Hubbard model (7):

$$\hat{H}_{\mathrm{HF}} = \sum_{ij\sigma} t_{ij}\hat{c}^{+}_{i\sigma}\hat{c}_{j\sigma} + \frac{U}{2}\sum_{i\sigma}\langle\hat{n}_{i-\sigma}\rangle\hat{n}_{i\sigma}. \tag{12}$$

According to the local force theorem, the exchange interaction is given by

$$J_{ij} = \frac{1}{2\pi S^2}\int_{-\infty}^{E_F} \mathrm{Im}(\tilde{V}_i G^{\downarrow}_{ij}\tilde{V}_j G^{\uparrow}_{ji})\, d\varepsilon, \tag{13}$$

here E_F is the Fermi level, $\tilde{V}_i = V_i^{\uparrow} - V_i^{\downarrow}$ denotes the spin-dependent Hartree-Fock potential calculated self-consistently, and $G^{\uparrow,\downarrow}(\varepsilon) = (\varepsilon - H^{\uparrow,\downarrow}_{\mathrm{HF}})^{-1}$ is the Green's function of the Hartree-Fock Hamiltonian. Unlike our approach (9), this formula requires presence of a magnetic order in the system.

In the case of the dimer, the exchange interactions obtained by using local force approach give excellent agreement with the spectrum of the Hubbard model for $\frac{t}{U} < 0.2$ (Fig. 2). For larger values of the hopping integrals, the averaged magnetic moment is strongly suppressed and becomes almost zero at $t/U \sim 0.5$. These results indicate the limits of the applicability of the mean-field Green's function approach for calculating the exchange interaction in strongly correlated systems.

IV. DIMER ON A SURFACE

The determination of the magnetic couplings in surface nanostructures is in the focus of the scanning tunneling microscopy experiments on these systems [37,38]. From the theoretical side, the experimental data can be simulated with Anderson impurity model approach [39]. In such simulations, the impurity-surface hybridization plays a principal role in formation of the electronic and magnetic properties of the

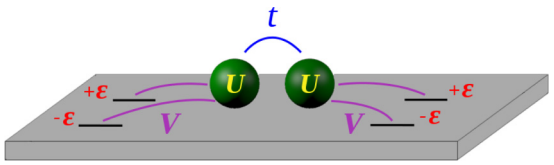

FIG. 3. Schematic representation of the dimer adsorbed on a substrate. Here, t and U are impurity kinetic and Coulomb repulsion terms whereas ε and V denote energy of bath states and hybridization terms, respectively.

surface nanosystems. In the case of a metallic surface, the hybridization can result in the valence fluctuations between different atomic configurations of the impurity [30,40]. Thus, the magnetic state of the impurity is a superposition of the states with different spins.

The developed method allows one to define the magnetic interaction in the regime of valence fluctuations. To demonstrate this, we perform the simulations for the dimer on a surface. Each correlated orbital of the dimer is connected to one empty and one occupied effective orbital of the substrate (Fig. 3) with energies $\epsilon_p = \pm\frac{U}{3}$. The hopping between impurities is fixed at the value of $t_{ij} = \frac{U}{100}$:

$$\hat{H}_{And} = \sum_i (\epsilon_i - \mu)\hat{n}_{i\sigma} + \sum_{ij\sigma} t_{ij}\hat{d}^\dagger_{i\sigma}\hat{d}_{j\sigma} + \frac{U}{2}\sum_{i\sigma}\hat{n}_{i\sigma}\hat{n}_{i-\sigma} + \sum_{p\sigma}\epsilon_p\hat{a}^\dagger_{p\sigma}\hat{a}_{p\sigma} + \sum_{ip\sigma}(V_{ip}\hat{d}^\dagger_{i\sigma}\hat{a}_{p\sigma} + \text{H.c.}), \quad (14)$$

where ϵ_i and ϵ_p are energies of the impurity and surface states, $d^\dagger_{i\sigma}$ ($d_{i\sigma}$) and $a^\dagger_{p\sigma}$ ($a_{p\sigma}$) are the creation (annihilation) operators for impurity and surface electrons, V_{ip} is the hopping integral between impurity and surface states, t_{ij} is the hopping integral between impurities, μ is the chemical potential, and U is the Coulomb repulsion.

Figure 4 shows, that at weak hybridization $\frac{V}{U} < 0.1$, the magnetic properties of the system are almost the same as for isolated $S = \frac{1}{2}$ dimer analyzed in the previous section. By increasing the hybridization of the impurity states, we amplify the valence fluctuations in the system and increase weights of the d^0 and d^2 configurations for each impurity. As a result, the local magnetic moment of the impurity is partially reduced. At the same time, there is a hybridization-induced magnetization of the bath states. Due to such a delocalization of the magnetic moment in the system, the dimer exchange interaction is strongly suppressed. It becomes almost zero at $\frac{V}{U} = 0.7$.

In the case of the multiorbital impurities on a metallic surface, the situation is more complicated. The valence fluctuations can lead to a superposition of different nonzero spin states for each impurity. For instance, in the case of the iron impurity on Pt(111) surface [30], there is a superposition of the $S = \frac{5}{2}$ (d^5 atomic configuration), $S = 2$ (d^6), and $S = \frac{3}{2}$ (d^7) spin states. Thus, the interimpurity magnetic interaction can be decomposed into partial contributions corresponding to couplings between different spin states of the impurities.

The results obtained for the dimer on a surface show that our method can be, in principle, combined with nano-DMFT [41] to probe magnetic excitations in correlated nanoscale devices such as molecules connected to electronic bath. On the other hand, the developed approach can be implemented in a cluster-DMFT [33] in which one solves a finite-size cluster embedded in a bath simulating the effect of the remaining part of an infinite lattice.

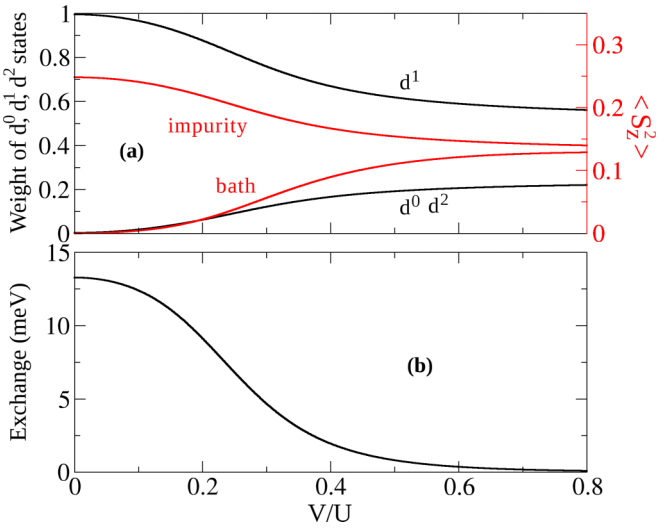

FIG. 4. (a) Contributions of d^0, d^1, and d^2 atomic states of the impurity to the ground state, the average value of square of the spin operator for impurity and bath orbitals. (b) Corresponding exchange constant derived with (9) for Anderson model (14) with two bath states at each impurity level (see Fig. 3).

V. SOLUTIONS FOR TRIANGLE AND TRIMER

Triangle is another example of the model for which we obtain excellent agreement of the electronic and spin eigenvalue spectra. The Heisenberg model spectrum for the triangle consists of fourfold degenerate ground and fourfold degenerate excited states (Fig. 5). As in the case of the dimer, the exchange interaction between spins in the triangle is defined by the corresponding splitting between excited- and ground-state levels. From Fig. 1 the Heisenberg model, which we constructed by using the HTE method, precisely reproduces the magnetic part of the Hubbard model.

Trimer. The situation becomes more complicated if we consider the trimer with the nearest-neighbor hopping presented in Fig. 6. In contrast to the triangle, the ground state of the trimer

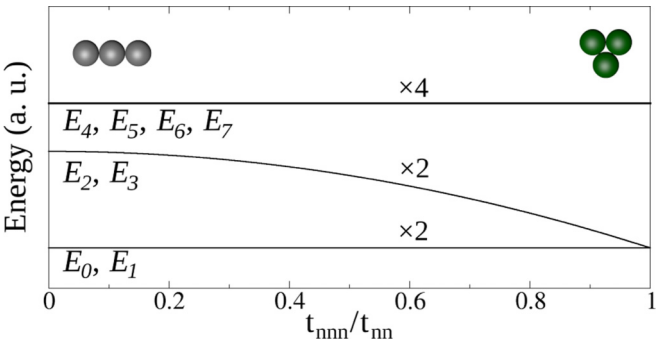

FIG. 5. Low-energy magnetic part of the Hubbard model eigenspectrum for trimer as a function of ratio $\frac{t_{nnn}}{t_{nn}}$. Numbers around the lines denote degeneracy of the corresponding energy levels. The spectra were calculated with $t_{nn} = 0.03$ eV and $\mu = \frac{U}{2} = 1.5$ eV.

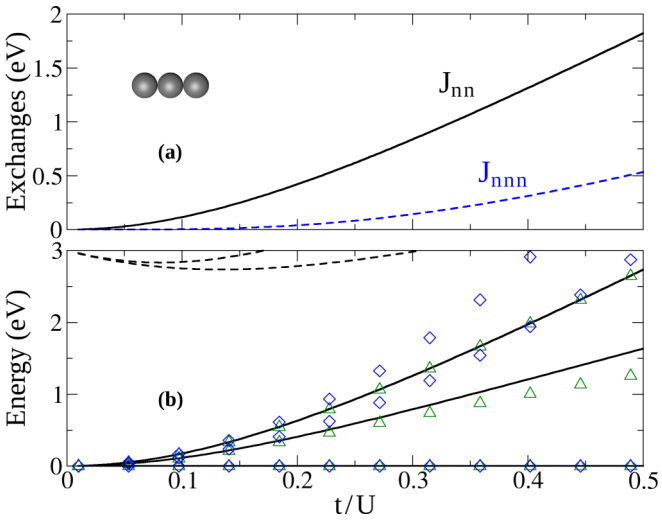

FIG. 6. (a) The calculated exchange interactions between nearest neighbors J_{nn} and next-nearest neighbors J_{nnn} in the trimer. (b) Comparison of the eigenvalue spectra for the trimer. Solid and dashed lines denote the Hubbard model spectrum. The symbols correspond to the Heisenberg model solutions with different sets of the exchange interactions and presented by blue rhombus (the Anderson's superexchange) and green triangles [the developed HTE method (9)].

is twofold degenerate (Fig. 5). In turn, the highest excited state in the magnetic part of the eigenspectrum is fourfold degenerate. As we will show below, the twofold intermediate excited level is related to the interaction between next-nearest neighbors.

For such hopping setup, within Anderson's superexchange theory we obtain the antiferromagnetic coupling $J_{ij} = \frac{4t_{ij}^2}{U}$ between nearest neighbors in the trimer. To define the interaction between next-nearest neighbors, one should use the fourth-order perturbation theory on the hopping. The situation becomes more complicated if the condition $t_{ij} \ll U$ is not fulfilled. On the other hand, by using the developed method (9) we obtain antiferromagnetic nearest- and second-nearest-neighbor exchanges. The solution of the corresponding Heisenberg model leads to perfect agreement between the spin and Hubbard model spectra up to large values of the ratio $\frac{t_{ij}}{U}$.

In the case of the trimer we can also explicitly relate the exchange interactions with the eigenvalues spectrum of the Hubbard model. For that, we used the condition $E_n^{\mathrm{Hubb}} - E_{n'}^{\mathrm{Hubb}} = E_n^{\mathrm{Heis}} - E_{n'}^{\mathrm{Heis}}$. Here, E_n^{Heis} is the eigenvalue of the Heisenberg model that can be found analytically (Appendix B). E_n^{Hubb} is the eigenvalue corresponding to the eigenstate from the low-energy (magnetic) part of the Hubbard Hamiltonian. The eigenvalue problem for Hubbard model was solved numerically. The structure of the low-energy part of the Hubbard model at different ratios between next-nearest hopping and nearest-neighbor one is presented in Fig. 5.

We obtain the following expressions for the magnetic couplings in the trimer:

$$\begin{aligned} J_{\mathrm{nn}} &= \tfrac{2}{3}(E_4 - E_0), \\ J_{\mathrm{nnn}} &= J_{\mathrm{nn}} - (E_2 - E_0), \end{aligned} \tag{15}$$

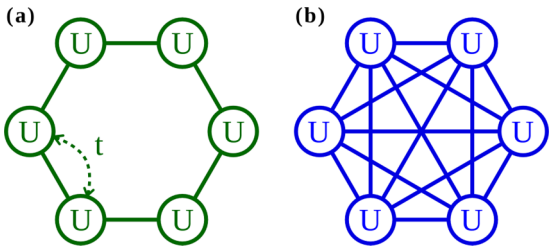

FIG. 7. Schematic representation of the hopping setups for the Hubbard Hamiltonian simulations. (a) The ring model with the nearest-neighbor hoppings. (b) All-to-all configuration in which all the hoppings between sites are equal.

where J_{nn} and J_{nnn} are exchange interactions between nearest neighbors and next-nearest neighbors in the trimer, respectively. One can see that the leading exchange interaction J_{nn} between the nearest neighbors is related to the energy splitting between ground state and highest excited state belonging to the magnetic part of the whole electronic spectrum. The situation with the next-nearest-neighbor coupling is more complicated. In addition to the $E_4 - E_0$ that is related to the leading exchange interaction, it also has the ferromagnetic contribution from the intermediate excited state $E_2 - E_0$. As we will show below, the similar picture is observed in quantum spin rings.

VI. QUANTUM SPIN RINGS

In this section, we present the results of computer simulations concerning the magnetic interactions in the finite quantum clusters with ring geometry. The theoretical interest in these systems is due to the synthesis and study of the magnetic properties of the molecular magnets with ring geometry [42–45]. Such systems demonstrate a number of interesting

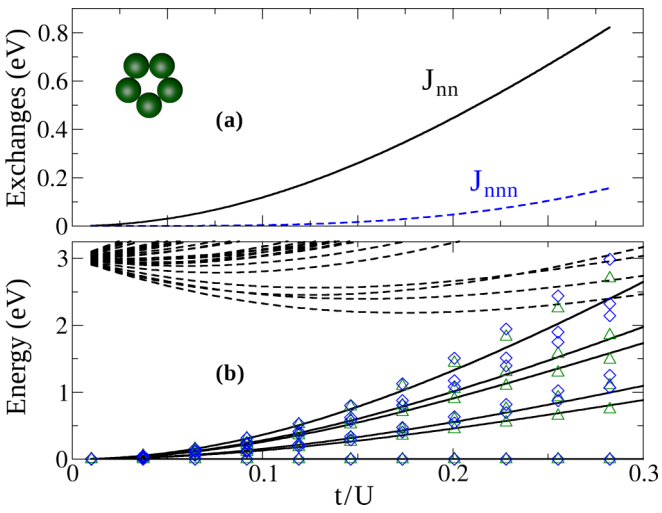

FIG. 8. (a) The calculated exchange interactions between nearest neighbors J_{nn} and next-nearest neighbors J_{nnn} in the five-site ring. (b) Comparison of the eigenvalue spectra for the five-site ring. Solid and dashed lines denote the Hubbard model spectrum. Blue rhombus and green triangles correspond to the Heisenberg model solutions with different sets of the exchange interactions: blue rhombus (Anderson's superexchange) and green triangles [developed method (9)].

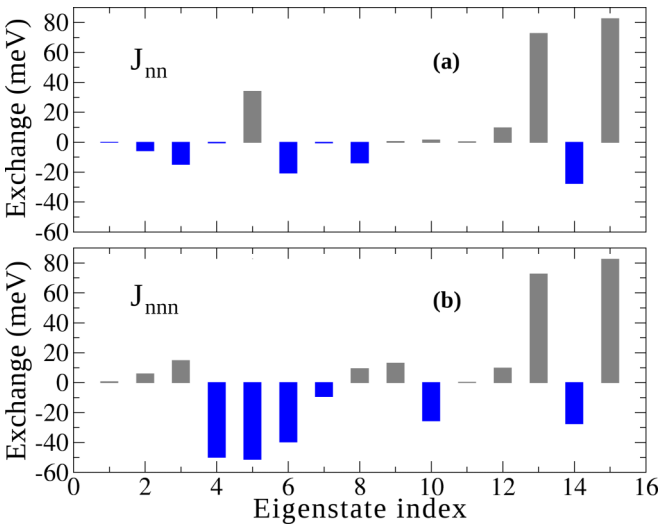

FIG. 9. Contributions from the different eigenstates of the Hubbard model to (a) the nearest-neighbor and (b) next-nearest-neighbor exchange interactions calculated for four-site ring with $t/U = 0.1$.

and complex phenomena, quantum spin tunneling, long-time spin relaxation, topological spin phases (Berry phases), and others. In this respect, the microscopic understanding of the intramolecular magnetic couplings plays a crucial role [46]. On the other hand, the spin rings are also of great practical interest since they can be used as building elements for novel quantum communication technologies [47] and for engineering quantum memory that is stable against noise and imperfections [48].

In our study, we have simulated the magnetic interactions in the quantum rings described by the Hubbard models with different hopping setups presented in Fig. 7. They can be realized in the quantum simulation experiments on ultracold atoms in optical lattices [49].

A. Rings with nearest-neighbor hoppings

First, we analyze the results of the simulations for quantum rings describing the Hubbard model with the only nearest-neighbor hopping integral. Similar to the case of the dimer and trimer, our method leads to better agreement between Heisenberg and low-energy Hubbard model spectra than the others. Figure 8 gives the comparison of the eigenvalues spectra calculated by different methods in the case of the five-site ring. One can see that the high-temperature expansion method reproduces the electronic Hamiltonian spectrum up to $t/U = 0.28$. At this value, the high- and low-energy parts of the spectrum overlap, which prevents us from determining the exchange interaction.

In the hopping setup we used [Fig. 7(a)], there are hopping integrals between nearest neighbors only. Nevertheless, each site has nonzero antiferromagnetic exchange interaction with all the other sites in the ring (we denote them J_{nnn}). Figure 8(a) demonstrates the behavior of such diagonal couplings at different t/U ratios in comparison with the leading exchange interaction between nearest neighbors J_{nn}. Despite of the fact that the coupling J_{nnn} grows much slower than the nearest-neighbor one it cannot be neglected when constructing the Heisenberg model at $t/U > 0.15$. It can be clearly seen from Fig. 8(b), in which the Anderson's superexchange theory with zero J_{nnn} leads to the eigenvalue spectrum deviating from the Hubbard model one.

The expression for the paramagnetic exchange interaction [Eq. (9)] that we derived contains the summation of the eigenstates belonging to the low-energy magnetic part of the Hubbard model spectrum. It is important to analyze the contribution of the individual eigenstates to the resulting exchange interaction. From Fig. 9 one can see that there are ferromagnetic contributions that partially compensate the antiferromagnetic ones. Interestingly, the contributions from the highest excited states are almost the same for the J_{nn} and J_{nnn} couplings. As it was shown in the case of the trimer, the intermediate excited eigenstates produce the ferromagnetic contributions to J_{nnn}.

B. Rings with all-to-all hoppings

By the example of the results for the five-site ring presented in Fig. 8(b) one can see that the quantum rings with nearest-neighbor hopping demonstrate rather complicated spectra. However, for practical purposes, for instance, to construct a quantum logic device, we need a system with the excitation spectrum as simple as possible. In the case of the quantum rings that we consider, the excitation spectrum can be considerably simplified by introducing the same hopping integral for all the bonds in the quantum Hamiltonian. It is the so-called all-to-all hopping configuration [Fig. 7(b)].

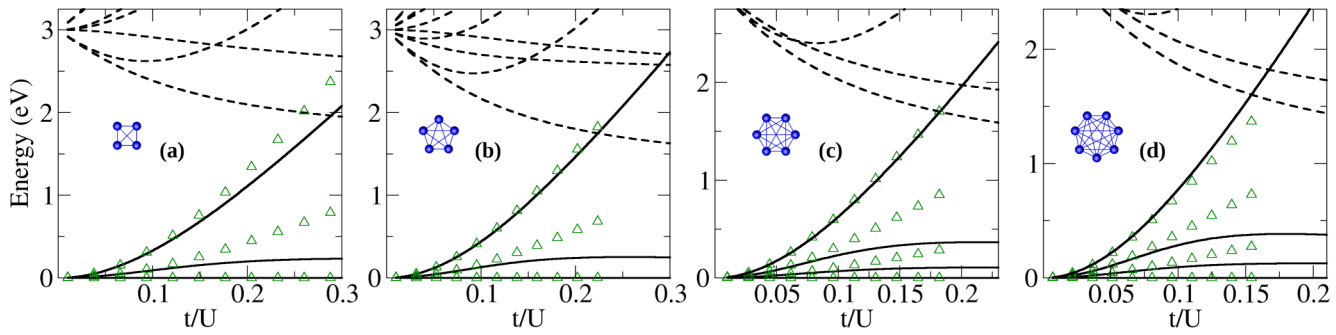

FIG. 10. Excitation spectra of all-to-all systems. Solid and dashed lines denote the Hubbard model spectrum. Green triangles correspond to the Heisenberg model solutions with the exchange interactions calculated by the high-temperature expansion method (9).

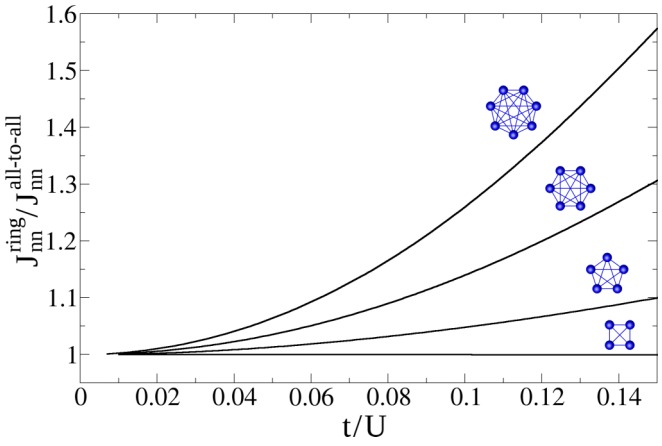

FIG. 11. The calculated ratio $\frac{J_{nn}^{ring}}{J_{nn}^{all\text{-}to\text{-}all}}$ demonstrating the contribution of the indirect hopping processes to the two-spin interaction.

The simplest Heisenberg Hamiltonian with two-spin exchange interactions constructed by the high-temperature expansion method gives the eigenvalue spectrum that is coincident with the Hubbard model one up to $t/U = 0.07$ (Fig. 10). For larger values of t/U we observe the deviation of the spin and electronic models that mainly concerns intermediate excited levels. The problem may be resolved by introducing the high-order multispin interactions (four-spin and six-spin) [21].

The pair exchange interaction between nearest neighbors in a quantum ring has the direct contributions, proportional to $t_{ij}t_{ji}$ and high-order nondirect ones, $\sum_k t_{ik}t_{kj}$, where the site index $k \neq i, j$. In case of the configurations with all-to-all hoppings, the nondirect processes become very efficient and strongly contribute to the exchange interaction between two spins. It can be seen from Fig. 11. For each pair in the N-site ring there are $N-2$ nondirect exchange path including one intermediate site.

VII. CONCLUSION

We propose the method for calculation of the magnetic interactions in the paramagnetic phase. Being formulated in the high-temperature and localized spin limits, our approach can be used for constructing the spin Hamiltonian in a wide range of the t/U ratios. It was shown by the classical examples such as the dimer and triangle finite clusters. By using the proposed method we investigated the magnetic couplings in quantum spin rings with different hopping configurations. Our methodological and calculation results will be useful for analysis of the data obtained in experiments with ultracold fermions that provide unique possibility to measure and control the spin-spin correlation function between two sites in optical lattice [49]. The proposed scheme can be also applied for simulating the magnetic couplings between impurities in metallic host. For that instead of the Hubbard model one should solve the two-impurity Anderson model.

ACKNOWLEDGMENTS

We acknowledge fruitful communications with M. Katsnelson, A. Lichtenstein, A. Secchi, A. Tsirlin, A. Katanin, S. Brener, I. Solovyev, and V. Anisimov. The work is supported by the grant program of the Russian Science Foundation Grant No. 15-12-20021. Modeling of the dimer on a surface (Section IV) was funded by the grant of the President of Russian Federation MD-6458.2016.2.

APPENDIX A: SPIN TRACES

The expansion of the spin-spin correlation function in the high-temperature limit [Eq. (3)] contains traces over spin operators. Here, we derive the exact expressions for these traces.

The expression $\mathrm{Tr}(\hat{S}_i^z \hat{S}_j^z)$ is equal to zero, if $i \neq j$. To demonstrate this, we consider a spin-$\frac{1}{2}$ system

$$\begin{aligned}\mathrm{Tr}\left(\hat{S}_i^z \hat{S}_j^z\right) &= \sum_{m=0}^{N-1} \langle \phi_m | \hat{S}_i^z \hat{S}_j^z | \phi_m \rangle \\ &= \langle \dots \uparrow_i \dots \uparrow_j \dots | \hat{S}_i^z \hat{S}_j^z | \dots \uparrow_i \dots \uparrow_j \dots \rangle \\ &\quad + \langle \dots \uparrow_i \dots \downarrow_j \dots | \hat{S}_i^z \hat{S}_j^z | \dots \uparrow_i \dots \downarrow_j \dots \rangle \\ &\quad + \langle \dots \downarrow_i \dots \uparrow_j \dots | \hat{S}_i^z \hat{S}_j^z | \dots \downarrow_i \dots \uparrow_j \dots \rangle \\ &\quad + \langle \dots \downarrow_i \dots \downarrow_j \dots | \hat{S}_i^z \hat{S}_j^z | \dots \downarrow_i \dots \downarrow_j \dots \rangle \\ &= \left(\frac{1}{4} - \frac{1}{4} - \frac{1}{4} + \frac{1}{4}\right)(2S+1)^{L-2} = 0, \end{aligned} \tag{A1}$$

where $|\phi_m\rangle$ are basis functions of Heisenberg model, L is the number of sites on the corresponding Heisenberg model, and S is the total value of spin on each site. In this way, it is possible to derive $\mathrm{Tr}(\hat{S}_i^z \hat{S}_j^z) = 0$ for $i \neq j$ in the general case for arbitrary spin S.

Further, for $i = j$ one can represent the trace equation (5) as

$$\mathrm{Tr}\left(\hat{S}_i^z \hat{S}_i^z\right) = (2S+1)^{L-1} \sum_{n=0}^{2S} (S-n)^2. \tag{A2}$$

The summation in Eq. (A2) could be easily expanded with arithmetic progression rules and known expression for $\sum_n n^2$ (see Ref. [50]). It yields expression (5) in the main text.

Similarly to the above equation, the statement

$$\mathrm{Tr}\left(\hat{S}_i^z \hat{S}_j^z \sum_{p \neq q} J_{pq} \hat{\hat{S}}_p \hat{\hat{S}}_q\right) = J_{ij} \mathrm{Tr}\left(\hat{S}_i^z \hat{S}_j^z \hat{S}_i^z \hat{S}_j^z\right) \tag{A3}$$

arises from the fact that $p \neq q$ in Heisenberg Hamiltonian. Indeed, $p = i$ and $q = j$ is the only case when the corresponding trace does not vanish.

Then, the trace equation (A3) can be rewritten similar to Eq. (A2):

$$\begin{aligned}&\mathrm{Tr}\left(\hat{S}_i^z \hat{S}_j^z \hat{S}_i^z \hat{S}_j^z\right) \\ &\quad = (2S+1)^{L-2} \sum_{n,m=1}^{2S} (S-n)^2 (S-m)^2, \end{aligned} \tag{A4}$$

which can be converted to the resulting expression (6) by using the same consideration as in the case of Eq. (A2).

TABLE III. Eigenvalues and eigenvectors of the Heisenberg model for triangle and trimer.

	E_i^{triangle}	E_i^{trimer}	Ψ_i
E_7	$\frac{3J}{4}$	$\frac{1}{2}J_{\text{nn}}+\frac{1}{4}J_{\text{nnn}}$	$\lvert\uparrow\uparrow\uparrow\rangle$
E_6	$\frac{3J}{4}$	$\frac{1}{2}J_{\text{nn}}+\frac{1}{4}J_{\text{nnn}}$	$\frac{1}{\sqrt{3}}(\lvert\uparrow\uparrow\downarrow\rangle+\lvert\uparrow\downarrow\uparrow\rangle+\lvert\downarrow\uparrow\uparrow\rangle)$
E_5	$\frac{3J}{4}$	$\frac{1}{2}J_{\text{nn}}+\frac{1}{4}J_{\text{nnn}}$	$\frac{1}{\sqrt{3}}(\lvert\downarrow\downarrow\uparrow\rangle+\lvert\downarrow\uparrow\downarrow\rangle+\lvert\uparrow\downarrow\downarrow\rangle)$
E_4	$\frac{3J}{4}$	$\frac{1}{2}J_{\text{nn}}+\frac{1}{4}J_{\text{nnn}}$	$\lvert\downarrow\downarrow\downarrow\rangle$
E_3	$-\frac{3J}{4}$	$-\frac{3}{4}J_{\text{nnn}}$	$\frac{1}{\sqrt{2}}(\lvert\uparrow\uparrow\downarrow\rangle-\lvert\downarrow\uparrow\uparrow\rangle)$
E_2	$-\frac{3J}{4}$	$-\frac{3}{4}J_{\text{nnn}}$	$\frac{1}{\sqrt{2}}(\lvert\downarrow\downarrow\uparrow\rangle-\lvert\uparrow\downarrow\downarrow\rangle)$
E_1	$-\frac{3J}{4}$	$-J_{\text{nn}}+\frac{1}{4}J_{\text{nnn}}$	$\frac{1}{\sqrt{6}}(\lvert\uparrow\uparrow\downarrow\rangle+\lvert\downarrow\uparrow\uparrow\rangle-2\lvert\uparrow\downarrow\uparrow\rangle)$
E_0	$-\frac{3J}{4}$	$-J_{\text{nn}}+\frac{1}{4}J_{\text{nnn}}$	$\frac{1}{\sqrt{6}}(\lvert\downarrow\downarrow\uparrow\rangle+\lvert\uparrow\downarrow\downarrow\rangle-2\lvert\downarrow\uparrow\downarrow\rangle)$

APPENDIX B: SOLUTIONS OF HEISENBERG MODEL FOR TRIANGLE AND TRIMER

Here, we retrieve solutions of the Heisenberg model in the case of the timer and triangle. J_{nn} and J_{nnn} denote the exchange interactions between nearest neighbors and next-nearest neighbors in the trimer. If $J_{\text{nn}}=J_{\text{nnn}}$, this is the case of the triangle. The obtained eigenvalues and eigenvectors presented in Table III are used for analysis of the low-energy magnetic part of the corresponding Hubbard model (Sec. V).

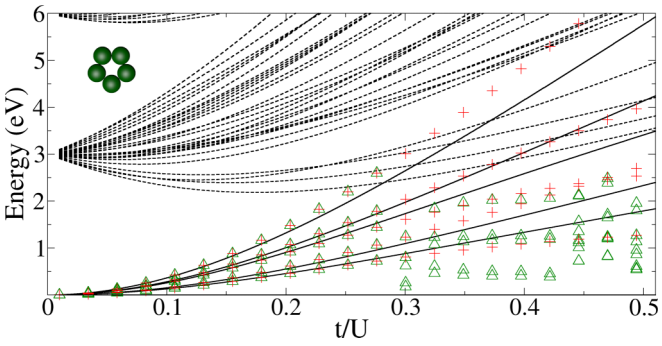

FIG. 12. Comparison of the eigenvalue spectra for the five-site ring. Solid and dashed lines denote the Hubbard model spectrum. Green triangles and red pluses denote Heisenberg model solutions obtained by using the developed method as described in Appendix C.

APPENDIX C: BEYOND THE CRITICAL RATIO $\frac{t}{U}$

Here, we analyze the situation when the magnetic and charge parts of the Hubbard eigenspectrum overlap. For this purpose, we use five-site ring system. From Fig. 12 the critical ratio $\frac{t}{U}$ for our method can be estimated as 0.27.

One can see that the exchange interaction calculated with Eq. (9) gives a spectrum (green triangles) that strongly deviates from that obtained for Hubbard model for $\frac{t}{U}>0.27$. The agreement between spin and electronic spectra can be partially restored, if one artificially excludes the states coming from the charge part of the whole spectrum (red pluses) in Eq. (9).

[1] R. M. White, *Quantum Theory of Magnetism* (McGraw-Hill, New York, 1970).

[2] A. Georges, G. Kotliar, W. Krauth, and M. J. Rozenberg, Rev. Mod. Phys. **68**, 13 (1996).

[3] M. I. Katsnelson and A. I. Lichtenstein, Phys. Rev. B **61**, 8906 (2000).

[4] S. Bhattacharjee, L. Nordström, and J. Fransson, Phys. Rev. Lett. **108**, 057204 (2012).

[5] A. Secchi, A. I. Lichtenstein, and M. I. Katsnelson, Ann. Phys. (NY) **360**, 61 (2015).

[6] A. I. Liechtenstein, M. I. Katsnelson, V. P. Antropov, and V. A. Gubanov, J. Magn. Magn. Mater. **67**, 65 (1987).

[7] Y. O. Kvashnin, O. Grånäs, I. Di Marco, M. I. Katsnelson, A. I. Lichtenstein, and O. Eriksson, Phys. Rev. B **91**, 125133 (2015).

[8] Y. O. Kvashnin, W. Sun, I. Di Marco, and O. Eriksson, Phys. Rev. B **92**, 134422 (2015).

[9] S. Keshavarz, Y. O. Kvashnin, I. Di Marco, A. Delin, M. I. Katsnelson, A. I. Lichtenstein, and O. Eriksson, Phys. Rev. B **92**, 165129 (2015).

[10] I. V. Solovyev, I. V. Kashin, and V. V. Mazurenko, Phys. Rev. B **92**, 144407 (2015).

[11] X. Wan, Q. Yin, and S. Y. Savrasov, Phys. Rev. Lett. **97**, 266403 (2006).

[12] W. Heisenberg, Z. Phys. **49**, 619 (1928).

[13] P. W. Anderson, Phys. Rev. **115**, 2 (1959); *Solid State Physics* (Academic, New York 1963), Vol. 14, p. 99 .

[14] J. W. D. Connolly and A. R. Williams, Phys. Rev. B **27**, 5169 (1983).

[15] A. V. Ruban, S. Shallcross, S. I. Simak, and H. L. Skriver, Phys. Rev. B **70**, 125115 (2004).

[16] S. Shallcross, A. E. Kissavos, V. Meded, and A. V. Ruban, Phys. Rev. B **72**, 104437 (2005).

[17] S. Miyahara and K. Ueda, J. Phys.: Condens. Matter **15**, R327 (2003).

[18] S. Lebernegg, A. A. Tsirlin, O. Janson, and H. Rosner, Phys. Rev. B **87**, 235117 (2013).

[19] A. A. Tsirlin, R. Nath, Ch. Geibel, and H. Rosner, Phys. Rev. B **77**, 104436 (2008).

[20] J. Stein, J. Stat. Phys. **88**, 487 (1997).

[21] H.-Y. Yang, A. M. Läuchli, F. Mila, and K. P. Schmidt, Phys. Rev. Lett. **105**, 267204 (2010).

[22] P. A. Igoshev, A. V. Efremov, A. I. Poteryaev, A. A. Katanin, and V. I. Anisimov, Phys. Rev. B **88**, 155120 (2013).

[23] P. A. Igoshev, A. V. Efremov, and A. A. Katanin, Phys. Rev. B **91**, 195123 (2015).

[24] Neil W. Ashcroft and N. David Mermin, *Solid State Physics* (Holt, Rinehart and Winston, Austin, TX, 1976).

[25] J. Hubbard, Proc. R. Soc. London, Ser. A **276**, 238 (1963).

[26] I. V. Solovyev, V. V. Mazurenko, and A. A. Katanin, Phys. Rev. B **92**, 235109 (2015).

[27] K. Yosida, *Theory of Magnetism* (Springer, Heidelberg, 1996).

[28] V. V. Mazurenko, S. N. Iskakov, M. V. Valentyuk, A. N. Rudenko, and A. I. Lichtenstein, Phys. Rev. B **84**, 193407 (2011).
[29] V. V. Mazurenko, S. N. Iskakov, A. N. Rudenko, I. V. Kashin, O. M. Sotnikov, M. V. Valentyuk, and A. I. Lichtenstein, Phys. Rev. B **88**, 085112 (2013).
[30] S. N. Iskakov, V. V. Mazurenko, M. V. Valentyuk, and A. I. Lichtenstein, Phys. Rev. B **92**, 245135 (2015).
[31] V. V. Mazurenko, M. V. Valentyuk, R. Stern, and A. A. Tsirlin, Phys. Rev. Lett. **112**, 107202 (2014).
[32] A. Vasiliev, O. Volkova, E. Zvereva, M. Isobe, Y. Ueda, S. Yoshii, H. Nojiri, V. Mazurenko, M. Valentyuk, V. Anisimov, I. Solovyev, R. Klingeler, and B. Büchner, Phys. Rev. B **87**, 134412 (2013).
[33] V. V. Mazurenko, A. I. Lichtenstein, M. I. Katsnelson, I. Dasgupta, T. Saha-Dasgupta, and V. I. Anisimov, Phys. Rev. B **66**, 081104(R) (2002).
[34] S. Trotzky, P. Cheinet, S. Fölling, M. Feld, U. Schnorrberger, A. M. Rey, A. Polkovnikov, E. A. Demler, M. D. Lukin, and I. Bloch, Science **319**, 295 (2008).
[35] D. Greif, M. F. Parsons, A. Mazurenko, C. S. Chiu, S. Blatt, F. Huber, G. Ji, and M. Greiner, Science **351**, 953 (2016).
[36] J. Stöhr and H. C. Siegmann, *Magnetism From Fundamentals to Nanoscale Dynamics* (Springer, Berlin, 2006).
[37] L. Zhou, J. Wiebe, S. Lounis, E. Vedmedenko, F. Meier, S. Blügel, P. H. Dederichs, and R. Wiesendanger, Nat. Phys. **6**, 187 (2010).
[38] C. F. Hirjibehedin, C. P. Lutz, and A. J. Heinrich, Science **312**, 1021 (2006).
[39] P. W. Anderson, Phys. Rev. **124**, 41 (1961).
[40] D. Novoselov, Dm. M. Korotin, and V. I. Anisimov, JETP Lett. **103**, 658 (2016).
[41] S. Florens, Phys. Rev. Lett. **99**, 046402 (2007).
[42] C. Delfs, D. Gatteschi, L. Pardi, R. Sessoli, K. Wieghardt, and D. Hanke, Inorg. Chem. **32**, 3099 (1993).
[43] R. Logemann, G. A. de Wijs, M. I. Katsnelson, and A. Kirilyuk, Phys. Rev. B **92**, 144427 (2015).
[44] K. Bärwinkel, H.-J. Schmidt, and J. Schnack, J. Magn. Magn. Mater. **212**, 240 (2000).
[45] J. Ummethum, J. Nehrkorn, S. Mukherjee, N. B. Ivanov, S. Stuiber, Th. Strässle, P. L. W. Tregenna-Piggott, H. Mutka, G. Christou, O. Waldmann, and J. Schnack, Phys. Rev. B **86**, 104403 (2012).
[46] V. V. Mazurenko, Y. O. Kvashnin, F. Jin, H. A. De Raedt, A. I. Lichtenstein, and M. I. Katsnelson, Phys. Rev. B **89**, 214422 (2014).
[47] S. Bose, B.-Q. Jin, and V. E. Korepin, Phys. Rev. A **72**, 022345 (2005).
[48] S. M. Giampaolo, F. Illuminati, A. Di Lisi, and S. De Siena, Laser Phys. **16**, 1411 (2006).
[49] D. Greif, G. Jotzu, M. Messer, R. Desbuquois, and T. Esslinger, Phys. Rev. Lett. **115**, 260401 (2015).
[50] G. A. Korn and T. M. Korn, *Mathematical Handbook for Scientists and Engineers: Definitions, Theorems, and Formulas for Reference and Review* (McGraw-Hill, New York, 1968).